

INTERACTION OF LASER RADIATION WITH MATTER. LASER PLASMA

PACS numbers: 41.75.Ht; 41.75.Jv; 52.38.Kd
DOI: 10.1070/QE2013v043n05ABEH015043

Double relativistic electron-accelerating mirror*

A.A. Andreev, K.Yu. Platonov

Abstract. **A numerical simulation of the interaction of a laser pulse with ultrathin targets has revealed a possibility of generating thin dense relativistic electron layers. The maximum kinetic energy of the electron mirror can be gained using an optimal combination of the target thickness and the laser pulse intensity and duration. It is proposed to use an additional (second) laser target, located at an optimal distance from the first target to cut off the laser pulse from the electron layer when the latter gains a maximum kinetic energy. This relativistic electron mirror can be used for efficient generation of 'hard' coherent radiation via counter reflection of an additional (probe) laser pulse from the mirror.**

Keywords: *laser acceleration of electrons, coherent X rays, ultrathin laser target, relativistic mirror.*

1. Introduction

Generation of short (with a wavelength shorter than the laser wavelength) dense relativistic electron bunches is urgent for studying and diagnosing ultrafast physical processes. These bunches allow for both direct electron microscopy and X-ray microscopy (through generation of short attosecond X-ray pulses) investigations. Short X-ray pulses also arise when additional laser pulses are scattered from electron bunches. Thin electron layers can be formed using different methods. For example, nonlinear oscillations of the electron density, excited in a laser target in the form of a gas jet, lead to generation of a sequence of thin electron bunches [1, 2]. Thin electron layers arise when a high-intensity p-polarised laser pulse is reflected from a solid target [3, 4]. Finally, when an intense laser pulse interacts with targets few micrometers thick, a rather thick (several hundreds of nanometres) bunch of fast electrons is generated at the rear side of the target [5]. As compared with these versions, an ultrathin graphene target [6] irradiated by a circularly polarised pulse has a number of advantages. First, since only one electron bunch is generated, its charge may be rather high (more than 1 nC). Second, one can easily control the bunch parameters (energy, thickness, number of particles) by changing the laser intensity, pulse duration, and graphene layer thickness.

In this study we performed numerical simulation of the interaction of a laser pulse with ultrathin targets to show a possibility of generating thin dense relativistic electron layers. The maximum electron energy is obtained at some optimal combination of the target thickness and the laser pulse intensity and duration. The optimal parameters are determined by solving the self-consistent system of Maxwell's equations and the equation of motion of a thin electron layer. To obtain maximally possible electron energies for thin relativistic layers, one needs an additional plasma target to cut off laser radiation from the plasma screen at the instant when the electron energy reaches a peak value. Scattering of a counter-propagating probe laser beam from the relativistic mirror formed makes it possible to generate 'hard' coherent electromagnetic radiation with a photon energy of several keV by converting the energy of the initial laser pulse generating an electron bunch with an efficiency of $\sim 0.1\%$.

2. Theoretical model of interaction between a thin electron layer and laser radiation

Numerical simulation shows that, when a linear polarised relativistic laser pulse irradiates an ultrathin (transparent) target, an electron bunch in the form of a thin flat layer is detached from the ion core and moves for a long time (as compared with the pulse duration) along with the electromagnetic wave. The detachment of a thin electron layer from a target was simulated using the two-dimensional PIC-code [7] for a thin carbon target (graphene). Figure 1 shows the spatial distributions of the electron density and laser field E_y at instants $t = 17$ and 33 fs after the onset of the pulse–target interaction. It can be seen that the first few periods of the laser pulse are sufficient to detach electrons from ions and to form a thin relativistic electron layer, propagating along with the laser pulse without diffusion in the longitudinal direction. Thus, the PIC simulation shows that an ultrathin laser target generates a thin one-dimensional relativistic electron layer moving along with the laser pulse. Note that the laser pulse leaves electrons behind at a distance of $\sim 2\gamma_x^2 c\tau_L$ (where γ_x is the bunch Lorentz factor and τ_L is the laser pulse duration), which has a macroscopic value on the order of few millimetres.

The motion of the electron layer is not equivalent to the motion of an individual electron in a wave, because a high concentration of electrons at some field point changes significantly the field structure at this point. Let us derive a system of equations taking into account this effect to describe the

*Presented at the Laser Optics Conference, St. Petersburg, Russia, June 2012.

A.A. Andreev S.I. Vavilov State Optical Institute, Birzhevaya liniya 12, 199034 St. Petersburg, Russia; St. Petersburg State University, Universitetskaya nab. 7, 199034 St. Petersburg, Russia;
e-mail: alexanderandreev72@yahoo.com;
K.Yu. Platonov S.I. Vavilov State Optical Institute, Birzhevaya liniya 12, 199034 St. Petersburg, Russia;
e-mail: konstantin_platonov@yahoo.com

Received 24 October 2012; revision received 19 February 2013
Kvantovaya Elektronika **43** (5) 435–442 (2013)
Translated by Yu.P. Sin'kov

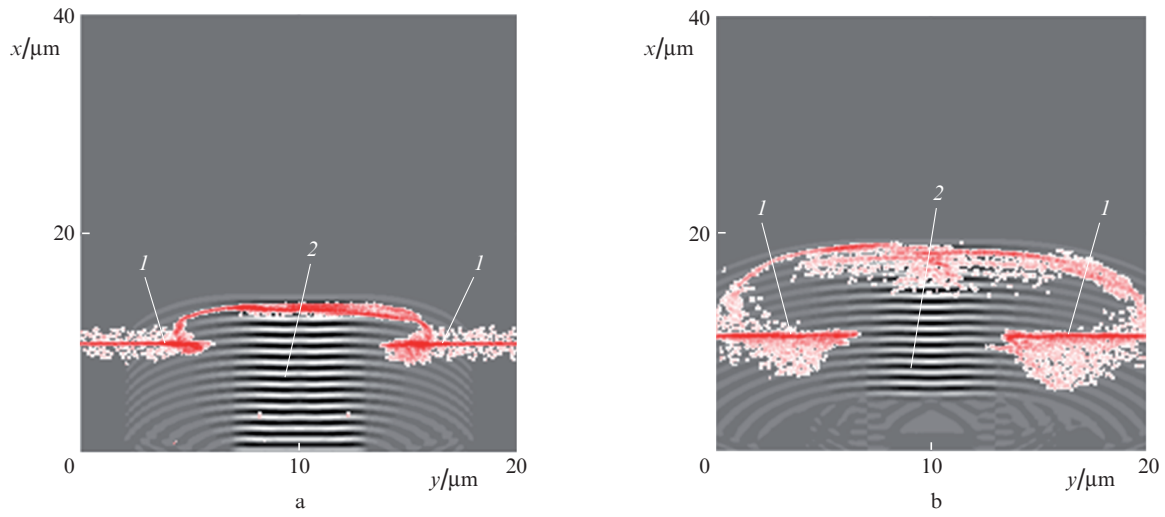

Figure 1. (*1*) Electron density and (*2*) laser field in the instants t = (a) 17 and (b) 33 fs for an ion concentration $n_i = 6 \times 10^{22}$ cm^{-3} in the carbon target at the target thickness 0.6 nm, laser pulse intensity 5×10^{19} W cm^{-2} ($a_0 > \varepsilon_0$), pulse duration 45 fs, laser-beam diameter 5 μm, and 10th-power transverse super-Gaussian profile. The calculation step is 0.05 nm at 40 particles per cell.

electron layer dynamics. In the one-dimensional spatial approximation and in the limit of infinitely thin electron layer (a case where the electron density distribution is described by a δ function), one can perform integration over the charge distribution in one-dimensional Lienard–Wiechert potentials, express the intrinsic fields of the layer in terms of its mechanical variables, and then write dynamic equations containing only the external field and electron layer velocities and coordinates. It is convenient to write the equations of motion of the layer in terms of the dimensionless variables P and Γ, which are integrals of motion for a single electron in an electromagnetic wave:

$$P = \frac{u_y}{\sqrt{1 - u_y^2 - \dot{X}^2}} - a_y^{\text{ext}}(\theta),$$
$$\Gamma = \frac{1 - \dot{X}}{\sqrt{1 - u_y^2 - \dot{X}^2}}, \tag{1}$$

where $a_y^{\text{ext}} = |e| A_y^{\text{ext}}(\theta)/(m_e c^2)$ is the dimensionless vector potential of the incident wave; $\theta = \omega t - kx$; and $u_y = v_y/c$ and $\dot{X} = v_x/c$ are the dimensionless components of the layer velocity along the polarisation direction (y) and the wave vector direction (x), respectively.

In these variables the equations of motion for a thin electron layer have the form

$$\frac{dP}{d\theta} = -\varepsilon_0 \frac{P + a_y^{\text{ext}}(\theta)}{\Gamma},$$
$$\frac{d\Gamma}{d\theta} = -2\varepsilon_0 \frac{[P + a_y^{\text{ext}}(\theta)]^2}{\Gamma^2 + [P + a_y^{\text{ext}}(\theta)]^2 + 1},$$
$$\frac{dX}{d\theta} = \frac{1 + [P + a_y^{\text{ext}}(\theta)]^2 - \Gamma^2}{2\Gamma^2}, \tag{2}$$
$$\frac{d\tau}{d\theta} = \frac{1 + [P + a_y^{\text{ext}}(\theta)]^2 + \Gamma^2}{2\Gamma^2},$$

where $\tau = \omega t$ and $X = \omega x/c$ are, respectively, the dimensionless time and layer coordinate and the dimensionless parameter $\varepsilon_0 = \pi n_e l_f/(n_{cr} \lambda_L)$ is determined by the target thickness l_f and the electron concentration n_e in it (n_{cr} is the critical concentration). Equations of motion (2) correspond to the equations of motion of an extended electron layer [8] when performing the transition $l_f \to 0$ in the latter and considering the motion of the central part of the layer.

Let the electron layer be immobile at the initial instant: $P(0) = 0$, $\Gamma(0) = 1$, $a_y^{\text{ext}}(0) = 0$, $X(0) = 0$, and $\tau(0) = 0$. Then a finite pulse ($a_y^{\text{ext}}(\theta) = a_0 \sin\theta$, $\theta \in [0; 2\pi N]$) acts on the layer and switches off after N periods. We will determine the final energy of the layer at $\theta = 2\pi N$, i.e., at the switch-off instant. This energy (the layer Lorentz factor) is expressed in terms of the variables P and Γ:

$$\gamma = \frac{1}{\sqrt{1 - u_y^2 - \dot{X}^2}} = \frac{1 + [P + a_y^{\text{ext}}(\theta)]^2 + \Gamma^2}{2\Gamma},$$
$$\gamma_x = \frac{1}{\sqrt{1 - \dot{X}^2}} = \frac{1 + [P + a_y^{\text{ext}}(\theta)]^2 + \Gamma^2}{2\Gamma\sqrt{1 + [P + a_y^{\text{ext}}(\theta)]^2}}. \tag{3}$$

Note that the layer energy determined by formula (3) coincides with the energy of an individual electron in a layer, because all electrons move identically in a thin layer.

For the case $\varepsilon_0 = 0$, where $P = 0$ and $\Gamma = 1$, formulas (3) yield the energy of an individual electron in a linearly polarised wave [9]:

$$\gamma = 1 + \frac{a_0^2 \sin^2\theta}{2}, \quad \gamma_x = \frac{1 + a_0^2 \sin^2\theta/2}{\sqrt{1 + a_0^2 \sin^2\theta}}. \tag{4}$$

After the end of the pulse ($\theta = 2\pi N$), a single electron, according to these formulas, retains its initial energy, and there is no energy exchange between the electron and the pulse. We will search for a solution to system (2) by increasing gradually the number of electrons in the layer (i.e., increasing the parameter ε_0, beginning with $\varepsilon_0 = 0$) and take values of laser parameters that can easily be implemented experimentally: $a_0 = 10$ and $N = 10$. The dependence of the layer energy at the end of the pulse on the layer thickness is shown in Fig. 2. At $\varepsilon_0 = 0$, the layer energy is determined by formulas (4). While ε_0 increases, the layer is accelerated, and its energy increases in comparison with the energy of an individual electron (4). At $\varepsilon_0 = 0.02$,

at the end of the pulse, the target is accelerated to energies greatly exceeding the individual-electron energy in a wave. The energy of a layer with a thickness $\varepsilon_0 = 0.02$ fluctuated during the pulse (see Fig. 3), and there was an instant when the Lorentz factor reached a value of 1600, which exceeded the finite value in Fig. 2. With an increase in the target thickness, beginning with certain ε_0 values for each laser intensity $I \propto a_0^2$, the electron layer stops being accelerated, and its energy undergoes stationary oscillations. For a target with $\varepsilon_0 = 0.03$ the pulse duration $N = 10$ is excessive, and the maximum energy can be gained using a shorter pulse. With a further increase in the layer thickness, stationary oscillations occur earlier, and the maximum layer energy decreases.

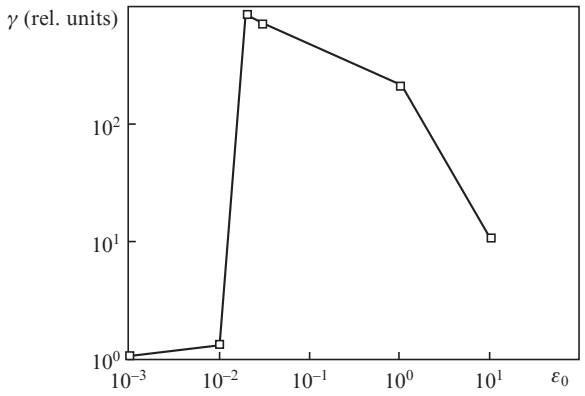

Figure 2. Layer energy at the end of the laser pulse as a function of its dimensionless thickness ε_0.

Thus, the equations of motion of the layer show that there is a layer thickness optimal for acceleration and that the instantaneous layer energy during the pulse may significantly exceed the energy at the pulse end. Therefore, when optimizing acceleration, it is expedient to interrupt somehow the pulse when the maximum energy is gained. As will be shown below (see Subsection 2.1), this can be done by fitting the pulse duration or installing a plasma mirror to cut off the laser field from electrons.

Note that the modulus of the exit angle (with respect to the x axis) of the electron layer from the laser field is described by the formula

$$\varphi = \arctan\frac{\sqrt{\gamma^2 - \gamma_x^2}}{\gamma\sqrt{\gamma_x^2 - 1}}. \qquad (5)$$

Despite the difference in the total and longitudinal Lorentz factors γ and γ_x (i.e., nonzero angle φ), formula (5) yields almost always (for relativistic electron layers) very small φ values, because the numerator is linear in γ, while the denominator is quadratic in γ. As a result, the electron layer moves virtually along the laser pulse propagation direction:

$$\varphi \approx \frac{\sqrt{1 - \gamma_x^2/\gamma^2}}{\gamma_x} \to 0 \quad \text{at} \quad \gamma_x \to \infty.$$

2.1. Single target

Let us determine [using Eqns (2)] the optimal thickness of the electron layer for gaining a maximum energy. We will impose the following limitations on the laser pulse and target parameters: the laser radiation intensity does not exceed 2×10^{21} W cm^{-2} ($a_0 = 30$) (the value that has been experimentally obtained to date), the target thickness is obviously larger than 0.1 nm (one-atom layer), and $n_e/n_{cr} > 100$ for almost any solid target. In this case, the lower boundary for the dimensionless thickness is $\varepsilon_0 \approx 0.004$. The results of calculations based on formulas (2), which are presented in Fig. 2, indicate that one should use small ε_0 values to obtain a maximum energy. To accelerate this target to an energy of 1 GeV, it is sufficient to use a pulse with $a_0 = 19$ and duration $N = 5$. At a wavelength $\lambda_L = 0.8$ μm the pulse intensity is 8×10^{20} W cm^{-2}. The energy dynamics of the electron layer accelerated by this pulse is shown in Fig. 3 as a function of the electromagnetic wave phase θ. It can be seen that a local energy maximum (1116 MeV) is attained at $\theta \approx 26$. However, the energy after the end of the pulse ($\theta = 10\pi \approx 31.4$) is only 245 MeV. The electron energy peak can be aligned with the end of the pulse by fitting the pulse duration and varying slightly the ε_0 value. For example, for a pulse with an intensity of 2×10^{21} ($a_0 = 30$) and duration $N = 4$, a target with $\varepsilon_0 = 0.0422$ has a maximum energy of 2.06 GeV, while the energy after four periods is 1.8 GeV, i.e., is close to maximum. However, this tuning is very sensitive to the exact thickness value: if $\varepsilon_0 = 0.005$ is taken to be 0.005 instead of 0.042, the output energy immediately drops to 306 MeV. Thus, the peak of the electron layer energy, which is bound to the end of the laser pulse, has a resonant character and its fixation calls for exact tuning of all parameters.

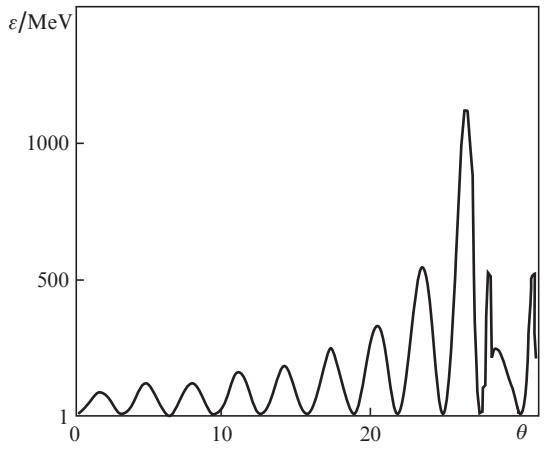

Figure 3. Electron layer energy ε as a function of the laser pulse phase θ.

Note that high electron energies at the output are obtained when the laser pulse is switched off sufficiently sharply. A consideration of a smooth (during two to four periods) switch off of the laser pulse yields only low output energies. For example, in the above example with $\varepsilon_0 = 0.042$, a replacement of a dramatically decreasing fragment of sinusoid

$$a_y^{ext}(\theta) = a_0 \sin\theta \; (\theta \in [0; 2\pi{\cdot}4])$$

with the smoother envelope

$$a_y^{ext}(\theta) = a_0 \sin\theta \sin^2(\theta/8) \; (\theta \in [0; 2\pi{\cdot}4])$$

leads to a decrease in both the maximum possible energy and the output energy. The latter is only ~60 MeV instead of 1.8 GeV. Real laser pulses, obtained without special technical tricks, are characterised by intensity rise and drop times on

the order of few periods, and the error in determining these times is larger than few tenths of a period. It is also difficult to monitor the target thicknesses on the order of few atomic layers. Therefore, it is extremely difficult to ensure stable intentional resonant tunings to the maximum layer energy after the end of interaction with a pulse in a real experiment. However, there is a possibility of preserving a local maximum value of the layer energy by installing a plasma screen (second target) at a certain point to cut off the laser field and retain the maximum layer energy [10, 11].

2.2. Double target

Let us now determine [based on Eqns (2)] the point of screen location and the laboratory time necessary to gain the maximum energy. The solution $\gamma(X)$ to system (2) is shown in Fig. 4. An energy of 1 GeV corresponds to the pulse phase $\theta \approx 26$ (see Fig. 3); in this case, the electron-layer coordinate is $X \approx 5 \times 10^4$. It can be seen that the electron energy peak is extended in the real coordinate space; therefore, there is no need for ultraprecise positioning of the plasma screen at high laser intensities and large Lorentz factors of the layer. The dimensionless coordinate $X \approx 5 \times 10^4$ corresponds to $x/\lambda_L = 7960$ or $x = 6.4$ mm. The error in positioning the second target (plasma mirror) of few tenths of millimetre is sufficiently small. The layer exit angle (5) at the maximum energy is only 0.1°. Thus, the plasma mirror allows one to fix a local time maximum for the layer energy.

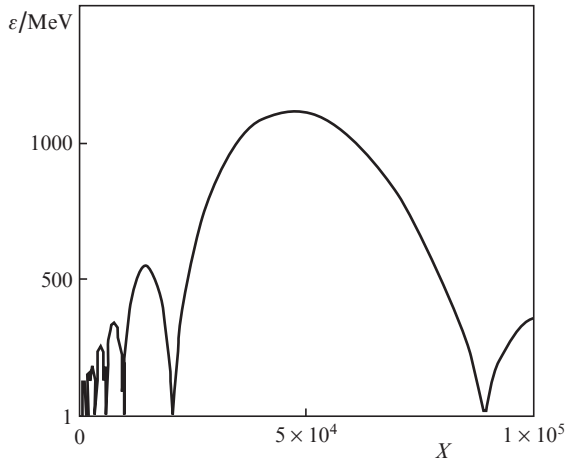

Figure 4. Dependence of the energy ε of the electron layer on its dimensionless longitudinal coordinate.

Note that a target with optimal ε_0 for obtaining the maximum energy γ of an electron in the layer is not optimal for gaining the maximum energy of the entire layer, i.e., the $\gamma\varepsilon_0$ value. With an increase in ε_0 this value first increases, reaches a maximum at $\varepsilon_0 \approx 0.1$, and then begins to decrease. The energy of an individual electron, corresponding to the maximum energy of the entire layer, is 558 MeV instead of 1 GeV. Thus, the target that is optimal with respect to the layer energy is thicker by a factor of about two than the target optimal with respect to γ, and the electron energy for this target is lower by a factor of about two. Note also that the maximum of the layer energy in ε_0 is sufficiently smooth, while γ depends more strongly on ε_0.

Analytical model (2) is valid for the one-dimensional case, ultrathin layer, and the absence of ions. Under experimental conditions, the electron layer is extracted from a target by a laser beam with a finite transverse size, as a result of which the model assumptions can be violated. Our two-dimensional simulation of the electron-layer generation (Fig. 1) and comparison of the layer energy with the theoretical predictions (Fig. 2) showed that the one-dimensional approximation adequately describes the thin layer dynamics.

Let us now show that the generated electron layer passes through the plasma screen (that cuts off the laser field) without significant energy loss and spatial-shape distortion.

3. Numerical simulation of the plasma-screen effect

The passage of electron layer through the plasma screen will be numerically simulated under the assumption that a laser pulse with an intensity of 10^{20} W cm^{-2}, duration 15 fs, and a sharp leading edge (with a laser beam diameter of 7 μm) interacts with two successively located targets, composed of C^{6+} ions with an initial concentration of 10^{23} cm^{-3}. The theoretical approaches to formation of a sharp leading edge for high-power pulses with durations of few periods were reported in [8] (see also references therein). Figures 5a and 5b show the initial arrangement of the targets. The first 5-nm-thick target is the source of electron layer and the second 1-μm target is a plasma screen, aimed at cutting off the laser pulse. The coordinate calculation step was taken to be 1 nm for 40 particles per cell. Figure 5a shows the spatial distribution of fast (with energies above 10 MeV) electrons at the instant $t = 35$ fs (before they enter the second target). It can be seen that a relativistic electron layer had been generated by that time. The cross section of the electron bunch by a plane $y = 9$ μm showed that the electron concentration in it is supercritical and amounts to 0.06 of the initial value (10^{23} cm^{-3}), while the bunch thickness is ~10 nm. The distribution function for all electrons in the calculation box is shown in Fig. 5c. The maximum energy for this distribution is determined by the formula $\gamma_1 = 1 + a_0^2/2$ and amounts to 20 MeV at $a_0 = 8.5$ ($\gamma = 38$). It can be seen in Fig. 5c that the maximum electron energy is ~28 MeV. This difference is explained by the increase in the field as a result of passage through the target. When the laser pulse arrives at the second target (plasma screen), the characteristic electron energy ($(\gamma_2 = (1 + a_0^2)^{1/2} \approx 8.6$) is 4.4 MeV; correspondingly, the distribution tail (Fig. 5c) should not change when passing through the second target, and the electrons with maximum energy should belong to the first target.

Figure 5b shows the electron density distribution (for electrons with energies exceeding 15 MeV) at the instant $t = 57$ fs, when the electron layer had passed through the second target. It can be seen that this passage was not accompanied by loss in energy and number of electrons. The laser pulse is completely cut off by the layer of dense plasma 1 μm thick. We should note (see also Fig. 1) that the electron bunch fills approximately the first five periods of the laser pulse; therefore, the calculation results (at a given target arrangement geometry) are valid at pulse durations $\tau_L \geqslant 13$ fs (the pulse is used only partially in this case). Longer pulses (for example, with $\tau_L = 45$ fs in Fig. 1) are called for at larger distances between the targets, when the light pulse leaves behind the electron bunch and the latter moves from the beginning to the end of the pulse.

Thus, the plasma screen makes it possible to separate efficiently a thin relativistic electron layer from a laser pulse with-

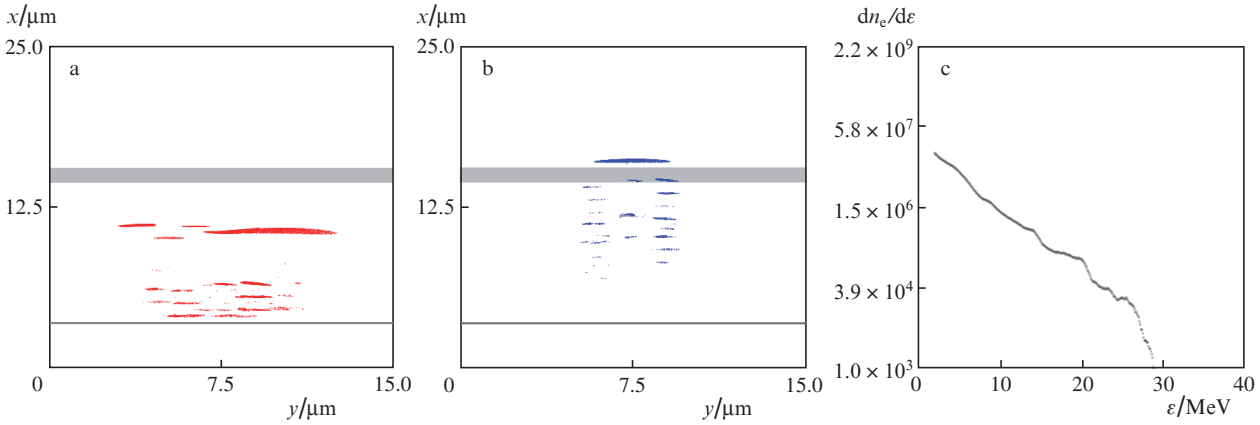

Figure 5. (a, b) Spatial distributions of all electrons at $t = 0$ (bright-grey bands) and fast electrons (with energies above 10 MeV) at t = (a) 35 fs (before arriving at the second target) and (b) 57 fs (for the electron layer passed through the second target) and (c) electron spectrum at $t = 35$ fs.

out loss in energy and number of electrons. Note that the thickness of the thus formed relativistic electron layer depends on the time profile of the laser pulse. For a pulse with a smooth leading edge (for example, a Gaussian pulse), the electron dynamics is significantly affected by the target ionisation. In the case of carbon atoms the first four levels become ionised when the laser intensity reaches $\sim 5 \times 10^{15}$ W cm^{-2} (10^{-5}–10^{-4} of the maximum value). Correspondingly, if a pulse has initially a sharp leading edge with this (or higher) intensity, the tunnel ionisation time is ~0.03 fs. These ionisation times do not affect the electron bunch thickness (~10 nm). At the same time, if the intensity of a Gaussian pulse is initially lower than 10^{14} W cm^{-2} (10^{-6} of the maximum), its pedestal (see the aforementioned range of intensities) successively ionises the electron shells of carbon, and ionisation lasts 5–10 fs. A spatially extended cloud of ionisation electrons is formed to be affected by the main part (peak) of the laser pulse.

A numerical simulation shows that the electron cloud is contracted to thicknesses of ~200–300 nm under these conditions. This thickness values can be explained as follows: during joint motion of electrons and a laser pulse (see Fig. 1) the electrons are concentrated near wave nodes (zero-field points), where the field energy density is minimum. The characteristic size of the node vicinity is on the order of 1/4 wavelength, a value determining the electron-layer thickness. Note that an electron bunch with a thickness smaller than the laser wavelength was observed at comparable parameters in experimental study [12]. A PIC simulation of the interaction of a short laser pulse with a thin target with allowance for the ionisation dynamics was performed in [13, 14]; this simulation also yielded thin (in comparison with the laser wavelength) electron bunches. A one-dimensional analytical model of this interaction was also constructed in [13].

Let us now consider the reflection of a probe counterpropagating laser pulse from electron mirrors of different thicknesses and densities and the generation of hard coherent electromagnetic radiation.

4. Reflection of a counterpropagating laser beam from a double relativistic electron mirror

The thus generated thin relativistic electron layer can be used as a source of coherent hard radiation, which arises as a result of scattering of a counterpropagating laser beam from this layer [15]. Simple estimates show the following: in the frame of reference where the layer is at rest (the rest frame), the frequency of the incident beam increases by a factor of $[(1 + \dot{X})/(1 - \dot{X})]^{1/2} \approx 2\gamma_x$ and it is reflected without changing frequency. Subsequent recalculation of the reflected radiation frequency in the initial laboratory frame of reference yields again a factor of $2\gamma_x$; hence, the photon energy in the reflected pulse is $\hbar\omega = 4\gamma_x^2 \hbar\omega_s$, where ω_s is the photon frequency in the incident counterpropagating beam. To estimate the reflection coefficient of a relativistic thin layer, we will use the well-known Fresnel reflection coefficient from a thin layer of immobile plasma $R' = \varepsilon_0'^2/(\varepsilon_0'^2 + 1)$ [16]. The surface electron concentration $n_e' l_f'$, which enters the expression for ε_0', is independent of the frame of reference; therefore, $n_e' l_f' = n_e l_f$.. Along with $n_e' l_f'$, the denominator of the expression for ε_0' contains only the incident radiation frequency ω_L', which is determined by the following relation in the rest frame:

$$\omega_L' = \omega_L[(1 + \dot{X})/(1 - \dot{X})]^{1/2} = (1 + \dot{X})\gamma_x^2.$$

As a result, the reflection coefficient, expressed in terms of the laboratory system variables, has the following form in the rest frame:

$$R' = \frac{\varepsilon_0^2}{\varepsilon_0^2 + (1 + \dot{X})^2\gamma_x^2} \approx \frac{\varepsilon_0^2}{\varepsilon_0^2 + 4\gamma_x^2}.$$

The number of scattered photons N_q (hard photons in the laboratory system) is expressed in terms of the number of incident laser photons N_s as $N_q = R'N_s$. Since the absolute numbers of photons are relativistic invariants, R' is also the reflection coefficient R in the number of photons (rather than in the pulse energy) in the laboratory system.

Note that the expression for the reflection coefficient R' implies the use of nonrelativistic (above 10^{18} W cm^{-2}) incident-radiation intensity I_s' in the rest frame. In the opposite case, as was shown in our previous study [12], the reflection coefficient decreases by a factor of $I_s'/10^{18}$ W cm^{-2} (a detailed and more complex formula for $R'(\varepsilon_0', I_L')$ was reported in [12]). This formula can be used for the reflection coefficient when the bunch thickness is smaller than the wavelength $\lambda_s' = \lambda_s/(2\gamma_s)$ of the radiation scattered in the rest frame. This approximation holds true for bunches several tens of nanometres thick, generated by pulses with a sharp leading edge. For bunches 200–300 nm thick (generated by Gaussian pulses), the reflection coefficient depends (with allowance for

the time dynamics of ionisation) on the bunch density distribution and is given by the formula

$$R_G = R'_G \approx \frac{\pi^2 e^4}{m_e^2 c^2 \gamma_x^4 \omega_s^2} \left| n'_e \frac{4\gamma\omega_s}{c} \right|^2,$$

where

$$n'_e(k) = \int n'_e(x') \exp(ikx') dx'$$

is the Fourier transform of the electron density of the bunch in its rest frame. The density distribution can be considered as Gaussian for estimates. The formulas used for the reflection coefficients imply also coherent character of reflection (this follows from the fact that R is proportional to n_e^2, i.e., the squared number of electrons in the layer). The condition for scattering coherence is given by the inequality

$$n_e \left(\frac{\pi c}{2\omega_s \gamma_x^2} \right)^3 > 1$$

for the thin-layer electron density at the instant of reflection. In the numerical simulation (the results of which are presented in Fig. 5), the electron density in the layer at $t = 57$ fs was 6×10^{21} cm^{-3}, and the above inequality was fulfilled in the entire range of electron energies (see Fig. 5c). If the electron density in the layer is low for a particular reason, i.e.,

$$n_e \left(\frac{\pi c}{2\omega_s \gamma_x^2} \right)^3 < 1,$$

coherent scattering will change to incoherent Thompson scattering from individual electrons. In this case, it is obvious that $N_q = N_s N_e \sigma_T / S = N_s \sigma_T n_e l_f$, where $N_e = n_e l_f S$; S is the scattering spot area, and $\sigma_T = 6.6 \times 10^{-25}$ cm^2 is the Thompson scattering cross section. The reflection coefficient in the case of incoherent scattering is $R_T = \sigma_T n_e l_f$, and its absolute values are smaller than those for coherent scattering.

An important characteristic of a hard-radiation source is its brightness B (the number of photons emitted from a unit area into a unit solid angle per unit time). At a laser pulse repetition rate $f \sim 10$ Hz (which is typical of the lasers under consideration) the average hard-radiation flux (number of photons per unit time) is $\Phi = fRN_s$. The average radiation brightness B in the layer propagation direction is related to the flux Φ by the expression [17]

$$B = \frac{10^{-6}}{S} \frac{3\gamma_x^2}{2\pi} \Phi = \frac{10^{-6}}{S} \frac{3\gamma_x^2}{2\pi} f N_s R, \qquad (6)$$

where B is in photons s^{-1} mm^{-2} mrad^{-2} per a spectral range with a width of 0.1% of the total spectrum width. In some studies [8] the peak brightness B_{max} during the scattering time $\tau_s/(4\gamma_x^2)$ (the number of pulse periods is retained upon scattering) of a single laser pulse of duration τ_s was considered instead of the average brightness (6). The peak brightness uses another definition for the hard-photon flux ($\Phi_{max} = 4\gamma_x^2 R N_s / \tau_s$) and exceeds the average brightness (6) by a factor of $4\gamma_x^2 (f\tau_s)^{-1}$. Below we present estimated values of the average brightness of a hard-radiation source, obtained by numerical simulation using formula (6).

Simple estimates of the reflection coefficient of a relativistic electron layer neglect some important physical effects arising during scattering, for example, deceleration of electrons by the counterpropagating beam. At low intensities and sufficiently thick targets not all electrons are extracted from the target by the laser pulse, and the parameter ε_0, which is proportional to the surface electron density in the moving electron bunch, depends on the laser intensity and the initial target thickness l_f. To calculate more strictly the energy of reflected photon and the reflection coefficient, we performed one-dimensional LPIC simulation of the reflection of a probe laser pulse (10^{18} W cm^{-2}, 16 fs) by a thin electron layer extracted from a 0.6-nm-thick C^{6+} target irradiated with a 16-fs laser pulse having an intensity of 5×10^{19} W cm^{-2}. When the electron layer moves in the summary field of two counterpropagating laser pulses of different amplitudes, the electron density is intensively diffused. To determine the reflection coefficient R and the frequency Ω (in units of initial frequency ω_s) of reflected radiation and the dependences of these parameters on the initial-target thickness and the main-pulse intensity, we performed similar calculations for intensities of 5×10^{18}, 10^{20}, and 5×10^{20} W cm^{-2} and for target thicknesses of 0.4, 1, 5, and 10 nm. The counterpropagating pulse had a constant intensity: 10^{18} W cm^{-2}.

The results of these calculations are shown in Fig. 6 in the form of dependences $R(I, l_f)$ and $\Omega(I, l_f)$. These dependences indicate that thin (less than 1 nm) laser targets and high (more than 10^{20} W cm^{-2}) intensities are optimal for generating hard ($\Omega > 100$) photons. The reflection coefficient for the probe pulse is small in this case: few percent. Knowledge of the reflection coefficient R allows one to find the conversion coefficient χ of the energy ε_L of the main laser pulse into hard radiation energy: $\chi = \Omega R \varepsilon_s / \varepsilon_L$, where ε_S is the energy of the scattered (falling on the moving electron layer) probe pulse. The opposite behaviour of the dependences of the reflection coefficient and the hard-photon energy on the laser intensity and target thickness in Fig. 6 indicates existence of optimal values of thickness and intensity, at which the conversion fac-

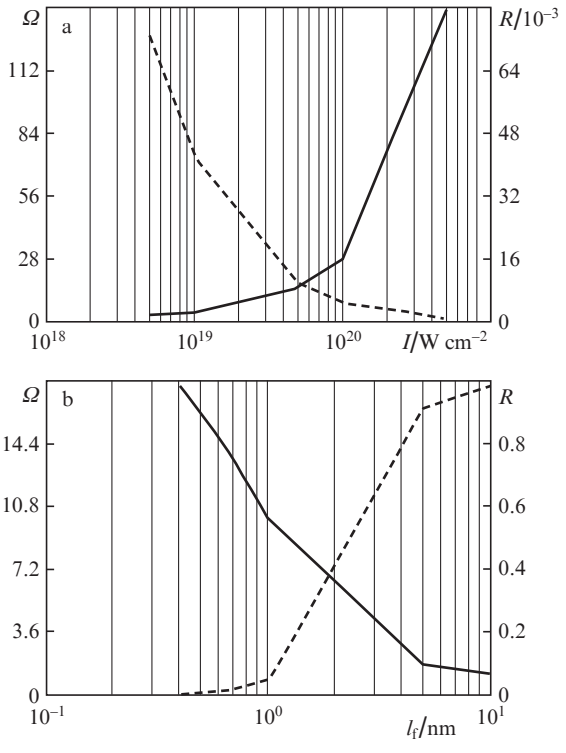

Figure 6. Dependence of the frequency of reflected hard radiation (solid lines) and reflection coefficient (dashed lines) on the (a) intensity I of the main laser pulse at a target thickness of 0.6 nm and (b) the initial target thickness at a laser intensity of 5×10^{19} W cm^{-2}.

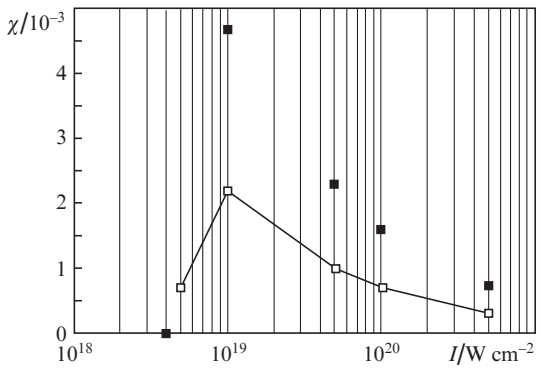

Figure 7. Dependence of the conversion coefficient of the main pulse energy into the energy of hard quanta on the laser intensity at a target thickness of 0.6 nm. Empty squares are the date of LPIC calculations, and dark squares are the estimates by the theoretical model.

tor χ reaches a maximum. Figure 7 shows a calculated (by means of LPIC simulation) dependence of the conversion factor on the laser intensity and theoretical estimates of χ, made on the assumption that all target electrons, independent of the target thickness and laser intensity, are extracted by the laser pulse ($\varepsilon_0 \propto Zn_i l_f$, where Z is the ionisation multiplicity and n_i is the ion concentration).

Comparison of this estimate with the results of LPIC simulation shows that the approximation considering all electrons as detached from the target is correct at high intensities. With a decrease in intensity, the conversion factor, calculated on the assumption that $\varepsilon_0 \propto Zn_i l_f$, increases to the intensity corresponding to the cutoff frequency Ω and then becomes zero (at low intensities $\Omega \to 1$ and it is incorrect to speak about conversion of optical photons into hard ones). The LPIC simulation data demonstrate that the conversion efficiency decreases at low intensities not only because of the frequency cutoff but also due to the decrease in the surface electron density in the moving bunch. The calculation data in Figs 6 and 7 indicate that optimum conversion is obtained at relatively low energies of hard photons: 20–40 eV ($\Omega \approx 10$–20); therefore, photons with high energies (exceeding 1 keV) are generated at a nonoptimal conversion factor in our case. The calculations for an intensity of 5×10^{19} W cm^{-2} and a 0.6-nm-thick carbon target yielded a conversion factor $\chi \approx 0.1\%$. This value exceeds, for example, the K_α-conversion factor in the same range of photon energies. Let us estimate the source brightness from formula (6) using the data in Fig. 6. The number of photons per unit area, N_s/S, at $\tau_L = 16$ fs, $I = 10^{18}$ W cm^{-2}, and $\lambda_L = 0.8$ μm is 5.3×10^{20} photons mm^{-2}. The reflection coefficient $R \approx 0.05$ and the frequency $\Omega = 4\gamma_x^2 \approx 40$. At a pulse repetition frequency $f = 10$ Hz the average brightness $B = 1.3 \times 10^{15}$ photons s^{-1} mm^{-2} mrad^{-2}. This value is much larger than the brightness of modern X-ray tubes (10^8 photons s^{-1} mm^{-2} mrad^{-2}) and laser-electron generators based on accelerators (10^{12} photons s^{-1} mm^{-2} mrad^{-2}) but smaller than the average brightness of modern synchrotrons (10^{21} photons s^{-1} mm^{-2} mrad^{-2}) in the same range of hard-photon energies. The reason for the loss in brightness in comparison with synchrotron sources is the small on–off time ratio of generated pulses. The peak brightness of the source reaches 3×10^{29} photons s^{-1} mm^{-2} mrad^{-2}, which is eight orders of magnitude higher than the synchrotron brightness. To increase the average brightness one can increase the interaction frequency between the probe pulse and the bunch, for example, by implementing repeated passes through the bunch or forming many bunches using an emitter composed of ultrathin targets. Since the reflection coefficient of an individual layer is $\sim 10^{-2}$, up to 100 layers can be used. The average brightness of this scheme is two orders of magnitude higher.

The above numerical estimates and simulation results are valid for a thin bunch (with a thickness smaller than the wavelength of scattered radiation in the rest frame) generated by a laser pulse with a sharp leading edge. For a 300-nm-thick bunch generated by a Gaussian pulse, with regard to ionisation, the average brightness decreases to 10^{11} photons s^{-1} mm^{-2} mrad^{-2} due to the reduction in the reflection coefficient (the electron bunch becomes transparent). The conversion factor χ also decreases by three orders of magnitude. In this case, to preserve high values of brightness and conversion factor, it is expedient to reflect long-wavelength laser radiation (for example, CO_2 laser radiation with a wavelength of 10.6 μm) from a bunch, for which the thin-layer approximation and reflection coefficient values at a level of few percent are retained at scattering. Here, the source brightness reaches 5×10^{15} photons s^{-1} mm^{-2} mrad^{-2} (due to the conservation of the reflection coefficient and the increase in the number of photons with lower energies) and the conversion factor remains at a level of several tenths of percent (0.3%).

Thus, the interaction of an intense relativistic laser pulse with an ultrathin target leads to generation of a thin dense relativistic electron layer. Using a plasma screen, one can fix a maximum value of the layer energy and use this layer to scatter a probe laser pulse and generate hard coherent electromagnetic radiation. The peak brightness of a source based on this scheme exceeds the brightness of existing hard-radiation sources by several orders of magnitude.

5. Conclusions

(1) To obtain maximum energy of thin electron layers, the optimal dimensionless thickness ε_0 of laser target should be much smaller than unity.

(2) The optimal target thickness ε_0 depends not only on the pulse intensity but also on the pulse duration. The optimal thicknesses for a pulse with a duration of 3 to 10 field periods are $\varepsilon_0 \sim 0.06$–0.02; the one-dimensional approximation remains valid in this case.

(3) At the end of the pulse the electron energy in the thin layer is not recovered to the initial value in the optimal range of thicknesses, in contrast to the energy of an individual electron in a plane electromagnetic wave. At the same time, the final value of the layer energy can be below the maximum value obtained during the laser pulse. Using the second target (plasma screen), one can fix the maximum layer energy. The spatial region where the layer energy reaches a maximum is rather extended; therefore, it is not necessary to position screen with a high accuracy; an error of several tenths of a millimetre is quite acceptable.

(4) The electron-layer thickness depends on the steepness of the laser pulse leading edge. Pulses with a sharp leading edge generate electron layers several tens of nanometres thick, even with allowance for the ionisation dynamics of target atoms. Gaussian pulses form (with allowance for the ionisation times) layers several hundreds of nanometres thick.

(5) Scattering of a counterpropagating probe laser beam from a relativistic mirror formed by the main beam makes it possible to generate hard coherent electromagnetic radiation with photon energies of several hundreds of electronvolts and

an efficiency of ~0.1% of the energy of the initial laser pulse generating the electron bunch.

(6) The peak brightness of the hard-radiation source based on the double-target scheme, exceeds the brightness of all existing hard-radiation sources by several orders of magnitude and its average brightness is higher than the brightness of X-ray tubes and laser-electron generators but lower than the brightness of synchrotron sources.

Acknowledgements. This work was supported by the Russian Foundation for Basic Research (Grant No. 09-02-12129-ofi_m).

References

1. Bulanov S. *Phys. Rev. Lett*., **91**, 085001 (2003).
2. Pirozhkov A. et al. *Phys. Plasmas*, **14**, 123106 (2007).
3. Naumova N. et al. *Phys. Rev. Lett*., **92**, 063902 (2004).
4. Andreev A. et al. *Proc. ICONO-LAT* (St. Petersburg, 2005).
5. Andreev A. et al. *Plasma Phys. Controlled Fusion*, **48**, 1605 (2006).
6. Kulagin V.V. et al. *Phys. Plasmas*, **14**, 113101 (2007).
7. Kemp A., Ruhl H. *Phys. Plasmas*, **12**, 033105 (2005).
8. Kulagin V.V. et al. *Phys. Rev. E*, **80**, 016404 (2009); **85**, 026405 (2012).
9. Landau L.D., Lifshits E.M. *The Classical Theory of Fields* (Oxford: Butterworth-Heinemann, 2000; Moscow: Fizmatgiz, 1976).
10. Miyauchi K., Kong Q., Andreev A., et al. *Phys. Plasmas*, **11**, 4878 (2004).
11. Wu H. et al. *Phys. Rev. Lett*., **104**, 234801 (2010).
12. Kiefer D., Henig A., Jung D. *Eur. Phys. J. D*, **55**, 427 (2009).
13. Bauer D. et al. *Phys. Rev. E*, **58**, 2436 (1998).
14. Glazyrin I.V., Karpeev A.V., Kotova O.G., Bychenkov V.Yu., Fedosejevs R., Rozmus W. *Proc. 39th EPS Conf. & 16th Int. Congress on Plasma Physics* (Stockholm, Sweden, 2012).
15. Ezirkepov T. et al. *Phys. Rev. Lett*., **103**, 025002 (2009).
16. Andreev A. et al. *Phys. Plasmas*, **17**, 123111 (2010).
17. Artyukov I.A. et al. Preprint No. 7/806, NIIYaF MGU (Skobeltsyn Institute of Nuclear Physics, Moscow State University) (Moscow, 2006).